Border collision bifurcations in two-dimensional piecewise smooth maps

Soumitro Banerjee*
Department of Electrical Engineering, Indian Institute of Technology, Kharagpur 721302, India

Celso Grebogi†
Institute for Plasma Research, Department of Mathematics and Institute for Physical Science and Technology, University of Maryland, College Park, Maryland 20742

(Received 10 August 1998; revised manuscript received 8 March 1999)

Recent investigations on the bifurcations in switching circuits have shown that many atypical bifurcations can occur in piecewise smooth maps that cannot be classified among the generic cases like saddle-node, pitchfork, or Hopf bifurcations occurring in smooth maps. In this paper we first present experimental results to establish the need for the development of a theoretical framework and classification of the bifurcations resulting from border collision. We then present a systematic analysis of such bifurcations by deriving a normal form — the piecewise linear approximation in the neighborhood of the border. We show that there can be eleven qualitatively different types of border collision bifurcations depending on the parameters of the normal form, and these are classified under six cases. We present a partitioning of the parameter space of the normal form showing the regions where different types of bifurcations occur. This theoretical framework will help in explaining bifurcations in all systems, which can be represented by two-dimensional piecewise smooth maps. [S1063-651X(99)05204-6]

PACS number(s): 05.45.−a

I. INTRODUCTION

Most studies in bifurcation theory have been done using smooth dynamical systems like the Hénon map, the Ikeda map, and the pendulum equation. In the class of nonsmooth systems, maps with square-root singularity have been studied extensively [1–4] because of their application in impact oscillators and other impacting mechanical systems. On the other hand, piecewise smooth maps with finite one-sided partial derivatives at the discontinuity have attracted relatively little attention. Though the possibility of strange bifurcations like period-2 to period-3 or period-2 to 18-piece chaotic attractor have been reported [5], no systematic study has been made to categorize the possible bifurcations in piecewise smooth maps. Such maps were considered to be just a mathematical possibility as no physical system with these characteristics was known.

However, in recent years there has been a discovery that a large class of engineering systems, particularly the switching circuits used in power electronics, yield piecewise smooth maps under discrete modeling, and border collision bifurcations are quite common in such systems [6,7]. This has provided motivation for the present study whose objective is to systematically analyze all different kinds of bifurcations that can occur in two-dimensional piecewise smooth maps.

We consider a general two-dimensional piecewise smooth map $g(\hat{x},\hat{y};\rho)$, which depends on a single parameter ρ. Let Γ_ρ, given by $\hat{x}=h(\hat{y},\rho)$ denote a smooth curve that divides the phase plane into two regions R_A and R_B. The map is given by

$$g(\hat{x},\hat{y};\rho)=\begin{cases} g_1(\hat{x},\hat{y};\rho) & \text{for } \hat{x},\hat{y}\in R_A \\ g_2(\hat{x},\hat{y};\rho) & \text{for } \hat{x},\hat{y}\in R_B . \end{cases} \tag{1}$$

It is assumed that the functions g_1 and g_2 are both continuous and have continuous derivatives. The map g is continuous but its derivative is discontinuous at the line Γ_ρ, called the ''border.'' It is further assumed that the one-sided partial derivatives at the border are finite. We study the bifurcations of this system as the parameter ρ is varied.

If a bifurcation occurs when the fixed point of the map is in one of the smooth regions R_A or R_B, it is one of the generic types, namely, period doubling, saddle-node, or Hopf bifurcation. But if a fixed point collides with the borderline, there is a discontinuous jump in the eigenvalue of the Jacobian matrix. In such a case, an eigenvalue may not ''cross'' the unit circle in a smooth way, but rather ''jumps'' over it as a parameter is varied continuously. One, therefore, cannot classify the bifurcations arising from such border collisions as those occurring for smooth systems where the eigenvalues cross the unit circle smoothly. In this paper we develop a classification for border collision bifurcations.

The paper is organized as follows. In Sec. II, we illustrate the problem with the help of an example of switching circuit. In Sec. III, the normal form is derived. In Sec. IV, we analyze the border collision bifurcations occurring in piecewise smooth maps. We present a partitioning of the parameter space of the normal form exhibiting various kinds of border collision bifurcations. We conclude in Sec. V.

II. EXAMPLES OF BORDER COLLISION BIFURCATIONS IN A POWER ELECTRONIC CIRCUIT

The subject of power electronics is concerned with high efficiency conversion of electric power, from the form avail-

*Author to whom correspondence should be addressed. Electronic address: soumitro@ee.iitkgp.ernet.in
†Electronic address: grebogi@chaos.umd.edu

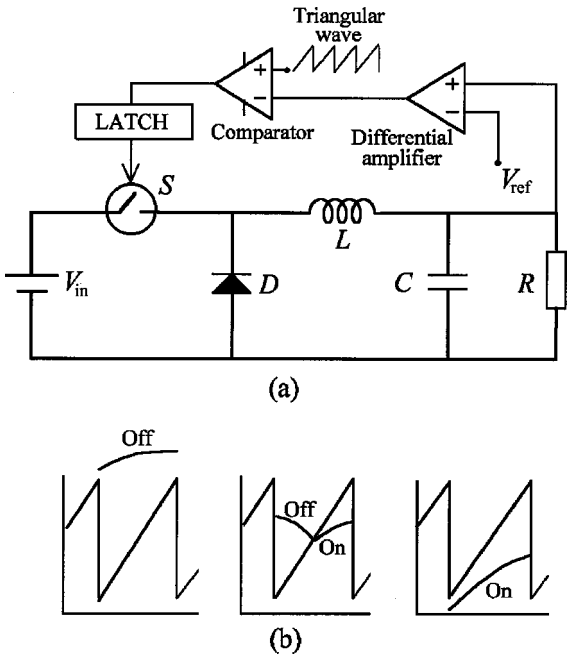

FIG. 1. (a) The buck converter with duty cycle controlled by voltage feedback and (b) the three ways the state can move from one sampling instant to the next.

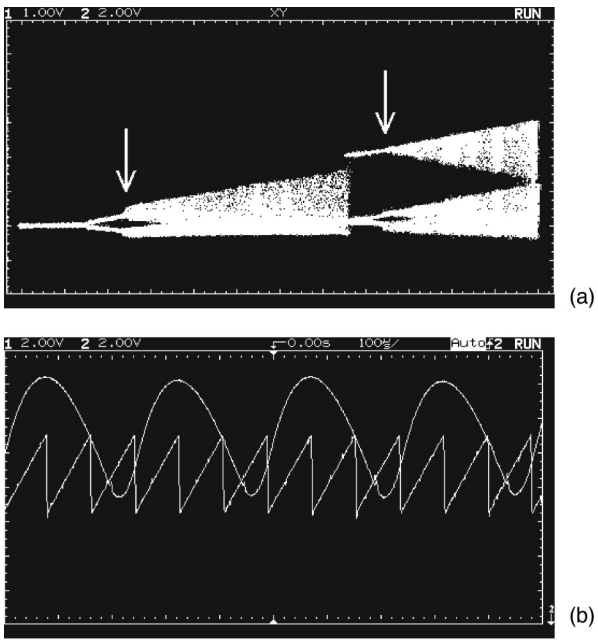

FIG. 2. Experimental bifurcation diagram of the buck converter. The parameter values are $R=23.5\ \Omega$, $C=5\ \mu$F, $L=2.96$ mH. Triangular wave: $V_U=8.43$V, $V_L=3.62$V, frequency 12 kHz. Bifurcation parameter V_{in} varied from 35 to 75 V.

able at the power source, to the form required by the specific appliance or load. Power electronic technology is increasingly finding application in the home and workplace: familiar examples are domestic light dimmers, fluorescent lamp ballasts, battery chargers, and switch-mode power supplies of all electronic appliances including the personal computer.

In contrast with mainstream electronics, power electronics is characterized by the use of electronic *switches*, which operate in an ''on'' or ''off'' state. Since electrical power supplies can be either dc or ac, there are four basic types of power converters: ac-dc, dc-ac, dc-dc, and ac-ac. Here we will consider one of the simplest but most useful of power converters — the dc-dc buck converter — which is used to convert a dc input to a dc output at a lower voltage.

The circuit diagram of the buck converter is shown in Fig. 1(a). The controlled switch S (generally realized by a MOSFET) opens and closes in succession, thus ''chopping'' the dc input into a square wave that alternates between the input voltage V_{in} and zero. The pulsed wave form is then low-pass filtered by a simple LC network, removing most of the switching ripple and delivering a relatively smooth dc output voltage v to the load resistance R. The diode D provides a path for the continuation of the inductor current during the *off* period. The dc output voltage can easily be varied by changing the duty ratio, i.e., the fraction of time that the switch is closed in each cycle.

In practice it is necessary to regulate v against changes in the input voltage and the load current. For example, if a buck converter is used to convert the standard 5-V dc supply used in computers to the 3.3 V needed for the Pentium CPU chip, it would be necessary to regulate the average output voltage at 3.3 V in spite of the varying power demand of the chip. This can be achieved by controlling the switch S by voltage feedback as shown in Fig. 1. In this simple proportional controller, a constant reference voltage V_{ref} is subtracted from the output voltage and the error is amplified with gain A to form a control signal $v_{con}=A(v-V_{ref})$. The switching signal is generated by comparing the control signal with a periodic sawtooth (ramp) wave form. S turns on whenever v_{con} goes below v_{ramp} and a latch allows it to switch off only at the end of the ramp cycle.

Though this circuit or its variants are used in a large number of practical applications requiring regulated dc power supply, it has been demonstrated [8–10] that the system can exhibit bifurcations and chaos for a large portion of the parameter space. To investigate the dynamics analytically, we obtain a two-dimensional Poincaré map by sampling the inductor current and capacitor voltage at the end of each ramp cycle.

Because of the transcendental form of the equations, the map cannot be determined in closed form. In simulation, the map has to be obtained numerically. It is, however, possible to infer the form of the map. There are three ways in which the system can move from one observation point to the next: (a) the control voltage is throughout above the ramp wave form and the switch remains off, (b) the cycle involves an *off* period and an *on* period, (c) the control voltage is throughout below the ramp wave form and the switch remains on. The three cases are shown in Fig. 1(b). These are represented by three different expressions of the map. The borderlines are given by the condition where the control voltage grazes the top and bottom of the ramp wave form. Therefore, there are three compartments in the phase space, separated by two borderlines, and we have a piecewise smooth map.

We present the experimentally obtained bifurcation diagrams for this system for different sets of parameter values.

An experimental bifurcation diagram is shown in Fig. 2(a). Here we find two parameter values (shown with arrows) for which a periodic orbit directly bifurcates into a chaotic orbit. Such bifurcations have been reported earlier in [8,11–

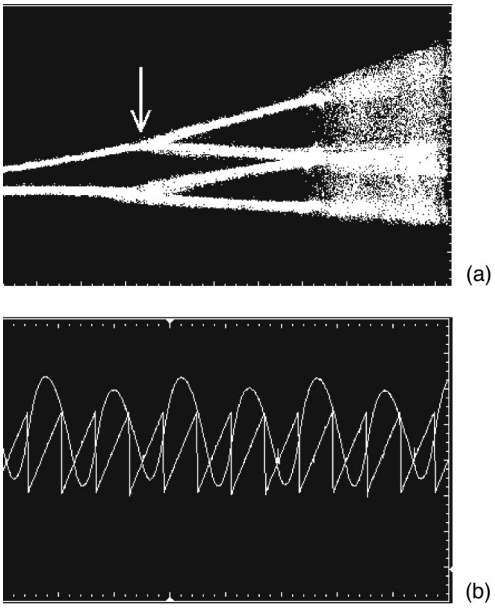

FIG. 3. Experimental bifurcation diagram of the buck converter. The parameter values are $R=28.9\ \Omega$, $C=5\ \mu$F, $L=2.96$ mH. Triangular wave: $V_U=8.43$V, $V_L=3.62$V, frequency 8 kHz. Bifurcation parameter V_{in} varied from 50 to 70 V.

13. The slight expansion of the attractor at the bifurcation point is due to system noise and can be ignored in theoretical studies. In Fig. 2(b) we present the continuous time plots of v_{con} and the triangular wave voltage at the bifurcation point shown by the second arrow, where a period-3 orbit bifurcates into a 3-piece chaotic orbit. It is seen that the v_{con} wave form grazes the top of the triangular wave, which means that a border collision bifurcation has occurred.

The distinguishing feature of this chaotic attractor is that there is no periodic window over a large range of the parameter value. We find from simulation that there are no coexisting attractors in this range. We say a chaotic attractor is *robust* if, for its parameter values there exists a neighborhood in the parameter space with no periodic attractor and the chaotic attractor is unique in that neighborhood [14]. The chaotic attractor resulting from this border collision is therefore robust. The question is, under what condition does robust chaos occur?

Another experimental bifurcation diagram for this system is shown in Fig. 3(a). The arrow shows a period doubling bifurcation, but the two bifurcated orbits do not diverge perpendicularly from the path of the fixed point before the critical parameter value. This is, therefore, not a standard pitchfork bifurcation. This kind of bifurcation has been reported in [15,16] also. Figure 3(b) gives the continuous time plots of v_{con} and the triangular wave voltage just after the bifurcation and shows that the period doubling occurred at a border collision. Again the question is, under what condition does this special type of period doubling occur?

It has been reported earlier [17] that this system has coexisting attractors for some ranges of parameter values. Since multiple attractors cannot be seen in experimental bifurcation diagrams, we present a numerically obtained bifurcation diagram in Fig. 4 showing the evolution of the main attractor and a coexisting attractor. It is found that the chaotic attractor comes into existence out of nothing at a particular parameter value. Under what condition can such strange bifurcations occur?

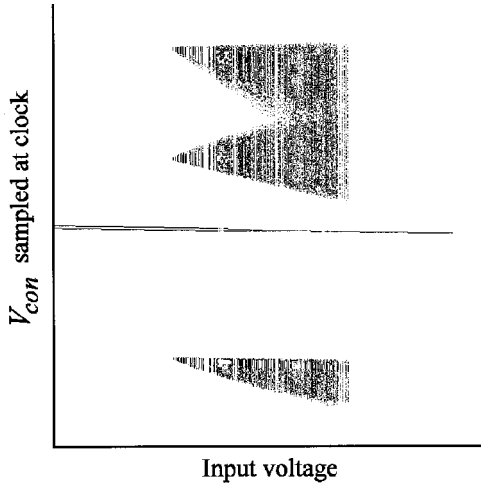

FIG. 4. Numerically obtained bifurcation diagram of the buck converter. The parameter values are $R=22\ \Omega$, $C=47\ \mu$F, $L=20$ mH. Triangular wave: $V_U=8.2$V, $V_L=3.8$V, time period 400 μs.

In the following sections we develop a complete theory of bifurcations in piecewise smooth maps, from which the answers to the above questions can be derived.

III. THE NORMAL FORM

Since the local structure of border collision bifurcations depends only on the local properties of the map in the neighborhood of the border, we study the border collision bifurcations with the help of ''normal forms'' — the piecewise affine approximations of g in the neighborhood of the border.

Define

$$\tilde{x}=\hat{x}-h(\hat{y};\rho),\quad \tilde{y}=\hat{y}.$$

This ρ-dependent change of variables moves the border to the $\tilde{y}$ axis. Then the map $g(\hat{x},\hat{y};\rho)$ can be written

$$g(\tilde{x}+h(\hat{y};\rho),\tilde{y};\rho)=f(\tilde{x},\tilde{y};\rho),$$

and the border is $\tilde{x}=0$. Suppose that when $\rho=\rho_0$ the map $f(\tilde{x},\tilde{y};\rho)$ has a fixed point P_0 on the border, that is,

$$\mathrm{P}_0=(0,\tilde{y}_0(\rho_0))=f(0,\tilde{y}_0(\rho_0);\rho_0).$$

Let e_1 be a tangent vector in the $\tilde{y}$ direction. The vector e_1 maps to a vector e_2. We assume e_2 is not parallel to e_1. Define the local coordinates as the following (cf. Fig. 5). Choose the point P_0 as the new origin for e_1 in the $\bar{y}$ direction and e_2 in the $\bar{x}$ direction. In these $\bar{x}$-$\bar{y}$ coordinates, the fixed point P_0 is given by (0,0), and the border Γ_ρ is given by $\bar{x}=0$. We define the new parameter $\bar{\mu}=\rho-\rho_0$ so that $\bar{\mu}_0=0$. Choose the scales such that at $\bar{\mu}=0$ a unit vector along the $\bar{y}$ axis maps to a unit vector along the $\bar{x}$ axis. The phase space is now divided into the two halves L and R and the map $f(\tilde{x},\tilde{y};\rho)$ can be written as $F(\bar{x},\bar{y};\bar{\mu})$.

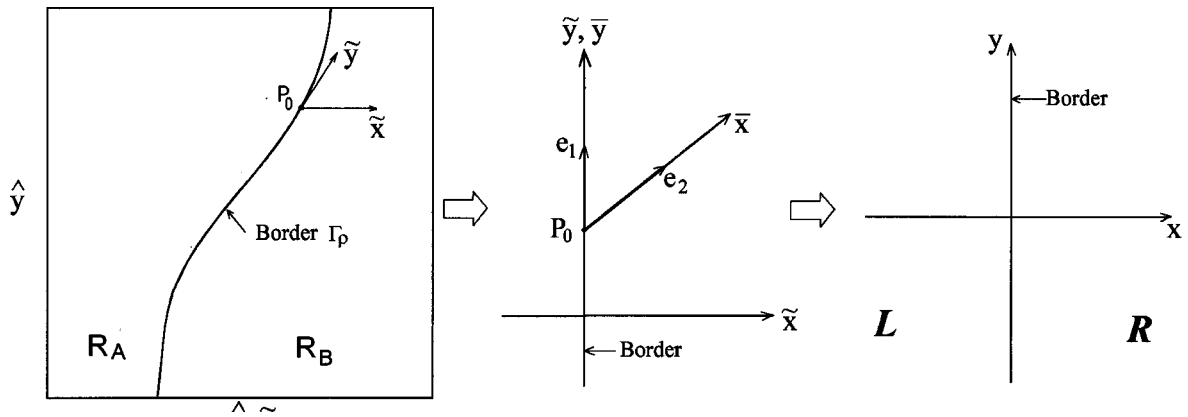

FIG. 5. The transformation of coordinates from the two-dimensional piecewise smooth map to the normal form.

We can write the map $F(\bar{\bar{x}},\bar{\bar{y}},\bar{\bar{\mu}})$ in the side L in the matrix form as

$$F(\bar{\bar{x}};\bar{\bar{y}};\bar{\bar{\mu}})=\begin{pmatrix} f_1(\bar{\bar{x}},\bar{\bar{y}};\bar{\bar{\mu}}) \\ f_2(\bar{\bar{x}},\bar{\bar{y}};\bar{\bar{\mu}}) \end{pmatrix}, \quad F(0,0;0)=\begin{pmatrix} 0 \\ 0 \end{pmatrix}.$$

Linearizing $F(\bar{\bar{x}},\bar{\bar{y}};\bar{\bar{\mu}})$ in the neighborhood of (0,0;0), we have

$$F(\bar{\bar{x}},\bar{\bar{y}};\bar{\bar{\mu}})=\begin{pmatrix} J_{11} & J_{12} \\ J_{21} & J_{22} \end{pmatrix}\begin{pmatrix} \bar{x} \\ \bar{y} \end{pmatrix}+\bar{\bar{\mu}}\begin{pmatrix} v_{Lx} \\ v_{Ly} \end{pmatrix}+o(\bar{\bar{x}},\bar{\bar{y}};\bar{\bar{\mu}}) \quad \text{for } \bar{x}\leqslant 0, \tag{2}$$

where

$$J_{11}=\lim_{\bar{x}\to 0^-,\,\bar{y}\to 0}\frac{\partial}{\partial x}f_1(\bar{\bar{x}},\bar{\bar{y}};0),$$

$$J_{12}=\lim_{\bar{x}\to 0^-,\,\bar{y}\to 0}\frac{\partial}{\partial y}f_1(\bar{\bar{x}},\bar{\bar{y}};0),$$

$$J_{21}=\lim_{\bar{x}\to 0^-,\,\bar{y}\to 0}\frac{\partial}{\partial x}f_2(\bar{\bar{x}},\bar{\bar{y}};0),$$

$$J_{22}=\lim_{\bar{x}\to 0^-,\,\bar{y}\to 0}\frac{\partial}{\partial y}f_2(\bar{\bar{x}},\bar{\bar{y}};0),$$

$$v_{Lx}=\lim_{\bar{x}\to 0^-,\,\bar{y}\to 0}\frac{\partial}{\partial \mu}f_1(\bar{\bar{x}},\bar{\bar{y}};0),$$

$$v_{Ly}=\lim_{\bar{x}\to 0^-,\,\bar{y}\to 0}\frac{\partial}{\partial \mu}f_2(\bar{\bar{x}},\bar{\bar{y}};0).$$

The particular choice of coordinates makes $J_{12}=1$ and $J_{22}=0$. Further, we note that J_{11} is the trace (denoted τ_L) and J_{21} is the negative of the determinant (denoted $-\delta_L$) of the Jacobian matrix. Thus Eq. (2) becomes

$$F(\bar{\bar{x}},\bar{\bar{y}};\bar{\bar{\mu}})=\begin{pmatrix} \tau_L & 1 \\ -\delta_L & 0 \end{pmatrix}\begin{pmatrix} \bar{x} \\ \bar{y} \end{pmatrix}+\bar{\bar{\mu}}\begin{pmatrix} v_{Lx} \\ v_{Ly} \end{pmatrix}+o(\bar{\bar{x}},\bar{\bar{y}};\bar{\bar{\mu}}) \quad \text{if } \bar{x}\leqslant 0. \tag{3}$$

Similarly, for side R we obtain

$$F(\bar{\bar{x}},\bar{\bar{y}};\bar{\bar{\mu}})=\begin{pmatrix} \tau_R & 1 \\ -\delta_R & 0 \end{pmatrix}\begin{pmatrix} \bar{x} \\ \bar{y} \end{pmatrix}+\bar{\bar{\mu}}\begin{pmatrix} v_{Rx} \\ v_{Ry} \end{pmatrix}+o(\bar{\bar{x}},\bar{\bar{y}};\bar{\bar{\mu}}) \quad \text{if } \bar{x}>0, \tag{4}$$

where the corresponding quantities in R are defined in a similar way.

Continuity of the map implies

$$\begin{pmatrix} v_{Lx} \\ v_{Ly} \end{pmatrix}=\begin{pmatrix} v_{Rx} \\ v_{Ry} \end{pmatrix}=\begin{pmatrix} v_x \\ v_y \end{pmatrix}.$$

We now make another change of variables so that the choice of axes is independent of the parameter. The coordinate transformation $x=\bar{x}$, $y=\bar{y}-\bar{\mu}v_y$, and $\mu=\bar{\mu}(v_x+v_y)$ [assuming $(v_x+v_y)\neq 0$] gives

$$G_2(x,y;\mu)=\begin{cases} \begin{pmatrix} \tau_L & 1 \\ -\delta_L & 0 \end{pmatrix}\begin{pmatrix} x \\ y \end{pmatrix}+\mu\begin{pmatrix} 1 \\ 0 \end{pmatrix} & \text{for } x\leqslant 0 \\ \begin{pmatrix} \tau_R & 1 \\ -\delta_R & 0 \end{pmatrix}\begin{pmatrix} x \\ y \end{pmatrix}+\mu\begin{pmatrix} 1 \\ 0 \end{pmatrix} & \text{for } x>0, \end{cases} \tag{5}$$

which is the desired 2D normal form.

Note that if $(v_x+v_y)=0$, then the fixed point moves along the border as μ varies. Hence we assume the genericity condition $(v_x+v_y)\neq 0$ to ensure that a border collision occurs at $\mu=0$.

It is interesting to note that τ_L and δ_L are simply the trace and the determinant of the Jacobian matrix of the fixed point P_0 on R_A side of the border Γ. Let P_ρ denote a fixed point of $g(\hat{x},\hat{y};\rho)$ defined on $\rho_0-\epsilon<\rho<\rho_0+\epsilon$ for some small $\epsilon>0$; then P_ρ depends continuously on ρ. Assume that P_ρ is in region R_A when $\rho<\rho_0$ and in region R_B when $\rho>\rho_0$, and that P_ρ is on Γ when $\rho=\rho_0$. For $\rho<\rho_0$, the eigenvalues of the Jacobian matrix of the fixed point P_ρ are denoted as λ_1 and λ_2. Since the trace and the determinant of the Jacobian

is invariant under the transformation of coordinates, we can obtain the values of τ_L and δ_L as

$$\tau_L = \lim_{\rho \to \rho_0^-} (\lambda_1 + \lambda_2),$$

$$\delta_L = \lim_{\rho \to \rho_0^-} (\lambda_1 \lambda_2). \tag{6}$$

The values of τ_R and δ_R can be calculated in a similar way for $\rho > \rho_0$. This property is very important in numerical computations. For a border-crossing periodic orbit with higher period, we examine the pth (if the period is p) iterate of the map. The matrices in Eq. (5) then correspond to the pth iterate rather than the first iterate of the map.

When δ_L and δ_R are zero, the system becomes one-dimensional and the normal form reduces to

$$G_1(x;\mu) = \begin{cases} a \quad x + \mu & \text{for } x \leqslant 0 \\ b \quad x + \mu & \text{for } x > 0, \end{cases} \tag{7}$$

where a and b are the slopes of the graph at the two sides of the border $x = 0$.

IV. CLASSIFICATION OF BORDER COLLISION BIFURCATIONS

Various combinations of the values of τ_L, τ_R, δ_L, and δ_R exhibit different kinds of bifurcation behaviors as μ is varied through zero. To present a complete picture, we break up the four-dimensional parameter space into regions with the same qualitative bifurcation phenomena. If the parameter combination is inside a region, then g and G_2 will have the same types of bifurcations. If it is on a boundary, then higher-order terms are needed to determine the bifurcations of g.

The fixed points of the system in both sides of the boundary are given by

$$L^* = \left(\frac{\mu}{1 - \tau_L + \delta_L}, \frac{-\delta_L \mu}{1 - \tau_L + \delta_L} \right),$$

$$R^* = \left(\frac{\mu}{1 - \tau_R + \delta_R}, \frac{-\delta_R \mu}{1 - \tau_R + \delta_R} \right),$$

and the stability of each of them is determined by the eigenvalues $\lambda_{1,2} = \frac{1}{2}(\tau \pm \sqrt{\tau^2 - 4\delta})$. If the eigenvalues are real, the slopes of the corresponding eigenvectors are given by $-(\delta/\lambda_1)$ and $-(\delta/\lambda_2)$, respectively. Since we consider only dissipative systems, we assume $|\delta_L| < 1$ and $|\delta_R| < 1$. For a positive determination there can be four types of fixed points. (1) When $\delta > \tau^2/4$, both eigenvalues of the Jacobian are complex, indicating that the fixed point is spirally attracting. If $\tau > 0$, it is a clockwise spiral, and if $\tau < 0$, the spiraling motion is counterclockwise. (2) When $\delta < \tau^2/4$, both eigenvalues are real. If $2\sqrt{\delta} < \tau < (1 + \delta)$, then the eigenvalues are positive and the fixed point is a regular attractor. If $-2\sqrt{\delta} > \tau > -(1 + \delta)$, then the eigenvalues are negative and it is a flip attractor. (3) If $\tau > 1 + \delta$, then $0 < \lambda_2 < 1$ and $\lambda_1 > 1$. The fixed point is a regular saddle. (4) If $\tau < -(1 + \delta)$, then $\lambda_2 < -1$ and $-1 < \lambda_1 < 0$. The fixed point is a flip saddle.

If the determinant is negative, there can be only two types of fixed points: (1) For $-(1 + \delta) < \tau < (1 + \delta)$, one eigenvalue is positive and the other negative—which means that the fixed point is a flip attractor. (2) For $\tau > (1 + \delta)$, $\lambda_1 > 1$ and $-1 < \lambda_2 < 0$, i.e., the fixed point is a flip saddle. If $\tau < -(1 + \delta)$, then $\lambda_2 < -1$ and $0 < \lambda_1 < 1$. The fixed point is again a flip saddle.

When referring to sides L and R, these quantities have the appropriate subscripts, i.e., $\lambda_{1L}, \lambda_{2L}$ are the eigenvalues in side L and $\lambda_{1R}, \lambda_{2R}$ are the eigenvalues in side R. As a fixed point collides with the border, its character can change from any one of the above types to any other. This provides a way of classifying border collision bifurcations.

It may be noted that in some portions of the parameter space there may be no fixed point in half of the phase space. For example, the location of L^* calculated by the above formula may turn out to be in side R. In such cases, the dynamics in L is determined by the character of the ''virtual'' fixed point. We denote such virtual fixed points by the overbar sign, as $\overline{L^*}$ and $\overline{R^*}$. If the eigenvalues are real, invariant manifolds of these virtual fixed points still exist and play an important role in deciding the system dynamics.

It should also be noted that if a certain kind of bifurcation occurs when μ is increased through zero, the same kind of bifurcation would also occur when μ is decreased through zero if the parameters in L and R are interchanged. Therefore, there exists a symmetry in the parameter space and in the following discussion it suffices to describe the bifurcations in half the parameter space. Moreover, we first consider the case of positive determinant, which constitutes a large class of physical systems. We take up the special features of systems with negative determinant at a later stage.

A special feature of the normal form (5) is that the unstable manifolds fold at every intersection with the x axis, and the image of every fold point is a fold point. The stable manifolds fold at every intersection with the y axis and the preimage of every fold point is a fold point. The argument is as follows. Forward iterate of points on the unstable manifold remain on the same manifold. In the normal form, points on the y axis map to points on the x axis. As an unstable manifold crosses the y axis, one linear map changes to another linear map. Therefore, the slope of the unstable manifold in the two sides of the x axis cannot be the same unless the parameters of the normal form in the two sides of the border are the same (implying a smooth map). In case of the stable manifold, the same argument applies for the inverse map. The inverse map of the normal form is given by

$$G_2^{-1}(x,y;\mu) = \begin{cases} \begin{pmatrix} 0 & -\dfrac{1}{\delta_L} \\ 1 & \dfrac{\tau_L}{\delta_L} \end{pmatrix} \begin{pmatrix} x \\ y \end{pmatrix} + \mu \begin{pmatrix} 0 \\ -1 \end{pmatrix} & \text{for } y > 0 \\ \begin{pmatrix} 0 & -\dfrac{1}{\delta_R} \\ 1 & \dfrac{\tau_R}{\delta_R} \end{pmatrix} \begin{pmatrix} x \\ y \end{pmatrix} + \mu \begin{pmatrix} 0 \\ -1 \end{pmatrix} & \text{for } y \leqslant 0. \end{cases} \tag{8}$$

Since its borderline is along the x axis, and points on the

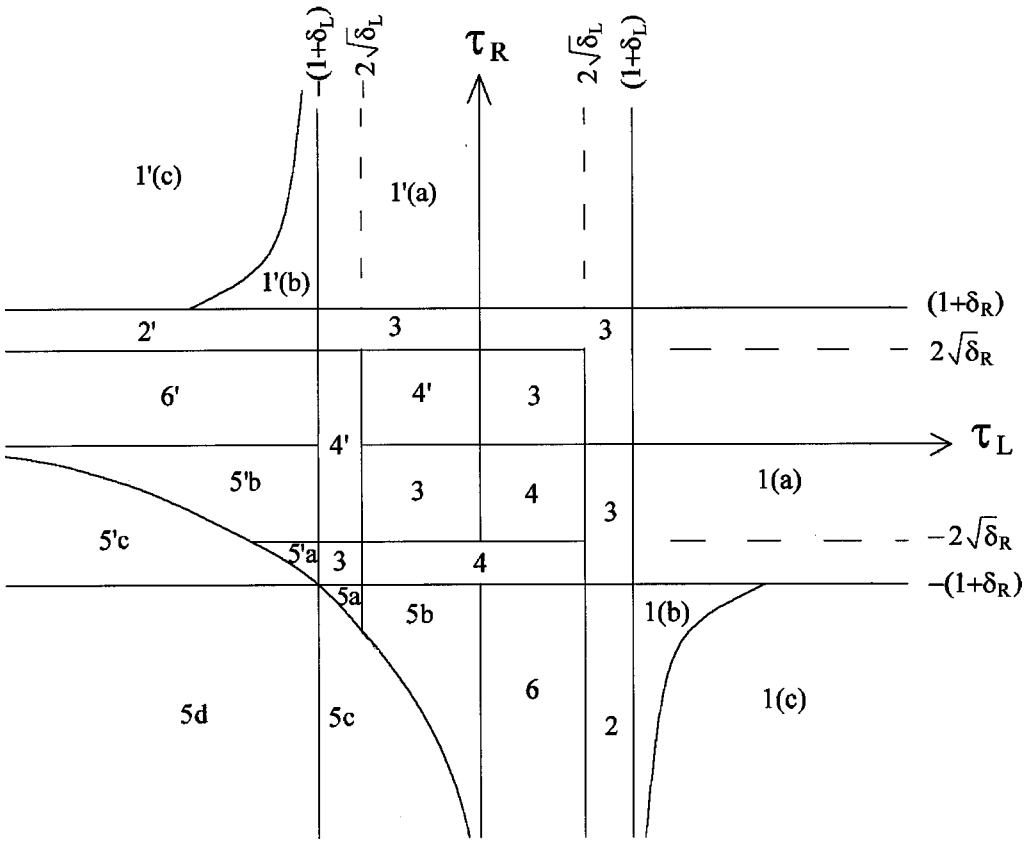

FIG. 6. The partitioning of the parameter space into regions with the same qualitative bifurcation phenomena. The numbering of the regions are the cases as discussed in the text. The regions shown in primed numbers have the same bifurcation behavior as the unprimed ones when μ is varied in the opposite direction.

x axis map to points on the y axis, we conclude that the stable manifold must have different slopes in the two sides of the y axis.

We now present the partitioning of the parameter space as shown in Fig. 6. The system behavior in the various regions of the parameter space are taken up in the following subsections.

A. Border collision pair bifurcation

Case 1. If

$$\tau_L > (1+\delta_L), \quad \tau_R < (1+\delta_R), \tag{9}$$

then there is no fixed point for $\mu<0$ and there are two fixed points, one each in L and R, for $\mu>0$. The two fixed points are born on the border at $\mu=0$. We call this a *border collision pair* bifurcation. An analogous situation occurs if $\tau_L < (1+\delta_L)$ and $\tau_R > (1+\delta_R)$ as μ is reduced through zero. Due to the symmetry of the two cases, we consider only the parameter region (9). There can be three types of border collision pair bifurcations depending on the character of the orbits for $\mu>0$.

Case 1(a). If $(1+\delta_R) > \tau_R > -(1+\delta_R)$, then R^* is stable. Therefore, it is like a saddle-node bifurcation, where a periodic attractor appears at $\mu=0$. There are two special features of this saddle node bifurcation. First, the fixed points are born on the border and move away from it as μ is increased. Second, there is no intermittency associated with this bifurcation.

Case 1(b). If

$$\tau_L > (1+\delta_L), \quad \tau_R < -(1+\delta_R), \tag{10}$$

$$\delta_L\tau_R\lambda_{1L} - \delta_R\lambda_{1L}\lambda_{2L} + \delta_R\lambda_{2L} - \delta_L\tau_R + \tau_L\delta_L - \delta_L^2 - \lambda_{2L}\delta_L > 0, \tag{11}$$

there is a bifurcation from no attractor to a chaotic attractor. The chaotic attractor for $\mu>0$ is robust [14].

Case 1(c). If $\tau_L > (1+\delta_L)$ and $\tau_R < -(1+\delta_R)$ and

$$\delta_L\tau_R\lambda_{1L} - \delta_R\lambda_{1L}\lambda_{2L} + \delta_R\lambda_{2L} - \delta_L\tau_R + \tau_L\delta_L - \delta_L^2 - \lambda_{2L}\delta_L \leqslant 0,$$

then there is an unstable chaotic orbit for $\mu>0$.

For Eq. (10), L^* is a regular saddle and R^* is a flip saddle. Let $\mathbf{U}_L$ and $\mathbf{S}_L$ be the unstable and stable manifolds of L^* and $\mathbf{U}_R$ and $\mathbf{S}_R$ be the unstable and stable manifolds of R^*, respectively. As shown earlier, $\mathbf{U}_L$ and $\mathbf{U}_R$ experience folds along the x axis, and all images of fold points are fold points. $\mathbf{S}_L$ and $\mathbf{S}_R$ fold along the y axis, and all preimages of fold points are fold points.

For condition (10), $\lambda_{1L} > \lambda_{2L} > 0$ and $0 > \lambda_{1R} > \lambda_{2R}$. The stable eigenvector at R^* has a slope $m_1 = (-\delta_R/\lambda_{1R})$ and the unstable eigenvector has a slope $m_2 = (-\delta_R/\lambda_{2R})$. Since points on an eigenvector map to points on the same eigenvector and since points on the y-axis map to the x axis, we conclude that points of $\mathbf{U}_R$ to the left of the y-axis map to

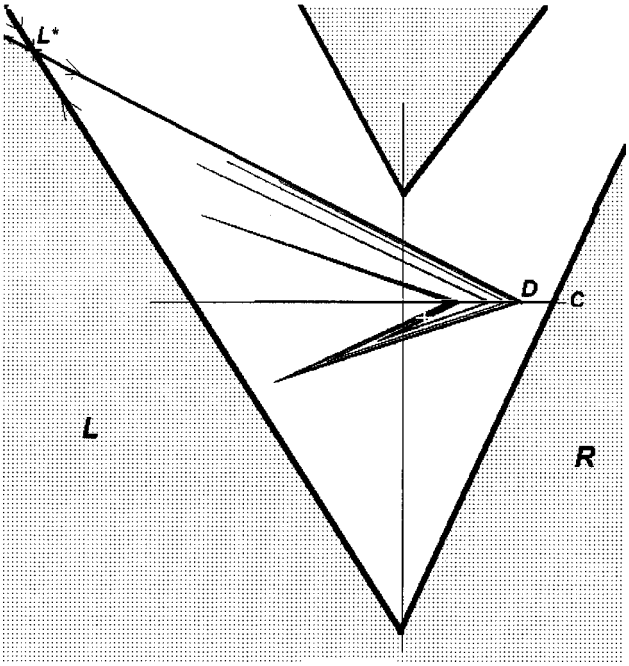

FIG. 7. The stable and unstable manifolds of L^* for $\tau_L=1.7$, $\delta_L=0.5$, $\tau_R=-1.7$, $\delta_R=0.5$. R^* is marked by the small cross inside the attractor.

points above the x axis. From this we find that $\mathbf{U}_R$ has an angle $m_3=(\delta_L\lambda_{2R})/(\delta_R-\tau_L\lambda_{2R})$ after the first fold. Under condition (10) we have $m_1>m_2>0$ and $m_3<0$. Therefore, there must be a transverse homoclinic intersection in R. This implies an infinity of homoclinic intersections and the existence of a chaotic orbit.

We now investigate the stability of this orbit. The basin boundary is formed by $\mathbf{S}_L.\mathbf{S}_L$ folds at the y axis and intersects the x axis at point C. The portion of $\mathbf{U}_L$ to the left of L^* goes to infinity and the portion to the right of L^* leads to the chaotic orbit. $\mathbf{U}_L$ meets the x axis at point D, and then undergoes repeated foldings leading to an intricately folded compact structure as shown in Fig. 7.

The unstable eigenvector at L^* has a negative slope given by $(-\delta_L/\lambda_{1L})$. Therefore, it must have a heteroclinic intersection with $\mathbf{S}_R$. Since both $\mathbf{U}_L$ and $\mathbf{U}_R$ have transverse intersections with $\mathbf{S}_R$, by the Lambda Lemma [18] we conclude that for each point q on $\mathbf{U}_R$ and for each ϵ-neighborhood $N_\epsilon(q)$, there exist points of $\mathbf{U}_L$ in $N_\epsilon(q)$. Since $\mathbf{U}_L$ comes arbitrarily close to $\mathbf{U}_R$, the attractor must span $\mathbf{U}_L$ on one side of the heteroclinic point.

Since all initial conditions in L converge on $\mathbf{U}_L$ and all initial conditions in R converge on $\mathbf{U}_R$, and since there are points of $\mathbf{U}_L$ in every neighborhood of $\mathbf{U}_R$, we conclude that the attractor is unique. This chaotic attractor cannot be destroyed by small changes in the parameters. Since small changes in the parameters can only cause small changes in the Lyapunov exponents, where the chaotic attractor is stable, it is also robust.

It is clear from this geometrical structure that no point of the attractor can be to the right of point D. If D lies towards the left of C, the chaotic orbit is stable. If D falls outside the basin of attraction, it is an unstable chaotic orbit or chaotic saddle. From this, the condition (11) of stability of the chaotic attractor is obtained. If $\delta_L=\delta_R=\delta$, this condition reduces to $\tau_R\lambda_{1L}-\lambda_{1L}\lambda_{2L}+\tau_L-\tau_R-\delta>0$.

B. Border crossing bifurcations

In all regions of the parameter space except Eq. (9), a fixed point crosses the border as μ is varied through zero. The resulting bifurcations are called *border crossing* bifurcations. In the following discussions we consider the bifurcations as μ varies from a negative value to a positive value.

Case 2. Regular attractor to flip saddle. This occurs if

$$2\sqrt{\delta_L}<\tau_L<(1+\delta_L), \qquad \tau_R<-(1+\delta_R).$$

There is a bifurcation from a period-1 attractor to a chaotic attractor as μ is increased through zero. This chaotic attractor is robust.

For $\mu<0$, L^* is a regular attractor while $\bar{R}^*$ is a flip saddle. All initial conditions in L converge on to L^*, while initial conditions in R converge on to $\mathbf{U}_R$. Since $\mathbf{U}_R$ must have a heteroclinic intersection with one of the stable manifolds of L, all initial conditions in R also converge on to L^*.

For $\mu>0$, R^* is a flip saddle. As shown in the discussion for Case 1(b), there is a homoclinic intersection in R implying the existence of a chaotic orbit. As $\bar{L}^*$ is in R, its stable manifolds point toward R. Since there is an intersection of $\mathbf{S}_R$ with the invariant manifold associated with λ_{1L}, all initial conditions converge on $\mathbf{U}_R$, making the chaotic attractor unique.

Case 3. There is a unique period-1 attractor for both positive and negative values of μ in the following cases. At border collision, only the path of the fixed point changes.

Regular attractor to spiral attractor: This occurs if

$$2\sqrt{\delta_L}<\tau_L<(1+\delta_L), \quad -2\sqrt{\delta_R}<\tau_R<2\sqrt{\delta_R}.$$

For $\mu<0$, all initial conditions in R are attracted to $\bar{R}^*$, which is in L. All initial conditions in L converge on to L^*. Therefore, the fixed point is the unique attractor. For $\mu>0$, all initial conditions in L move linearly towards $\bar{L}^*$, which is in R, and all points in R spiral towards R^*. Therefore, R^* is the unique attractor.

Spiral attractor to spiral attractor having the same sense of rotation: This occurs if

$$0<\tau_L<2\sqrt{\delta_L}, \quad 0<\tau_R<2\sqrt{\delta_R},$$

or

$$-2\sqrt{\delta_L}<\tau_L<0, \qquad -2\sqrt{\delta_R}<\tau_R<0.$$

If the spiraling orbits in L and R have the same sense, there is an overall spiraling orbit converging on the fixed point. Therefore, there is an unique period-1 attractor for both $\mu<0$ and $\mu>0$.

Regular attractor to regular attractor:

$$2\sqrt{\delta_L}<\tau_L<(1+\delta_L), \quad 2\sqrt{\delta_R}<\tau_R<(1+\delta_R).$$

Flip attractor to flip attractor:

$$-2\sqrt{\delta_L}>\tau_L>-(1+\delta_L), \quad -2\sqrt{\delta_R}>\tau_R>-(1+\delta_R).$$

Regular attractor to flip attractor:

$$2\sqrt{\delta_L}<\tau_L<(1+\delta_L), \quad -2\sqrt{\delta_R}>\tau_R>-(1+\delta_R).$$

In the above three cases, for $\mu<0$, initial conditions in R move linearly to $\bar{R}^*$. Since there must be a heteroclinic intersection of the stable manifolds, all initial conditions converge on L^*. The situation for $\mu>0$ is similar.

Case 4. In the following cases there can be bifurcation from multiple attractors to multiple attractors. There are general mechanisms for the occurrence of coexisting attractors.

Spiral attractor to spiral attractor with opposite sense of rotation: This occurs if

$$0<\tau_L<2\sqrt{\delta_L}, \quad -2\sqrt{\delta_R}<\tau_R<0,$$

or

$$-2\sqrt{\delta_L}<\tau_L<0, \quad 0<\tau_R<2\sqrt{\delta_R}.$$

Spiral attractor to flip attractor: This occurs if

$$-2\sqrt{\delta_L}<\tau_L<2\sqrt{\delta_L}, \quad -2\sqrt{\delta_R}>\tau_R>-(1+\delta_R).$$

There can be multiple attractors on both sides of μ, one of which is a fixed point.

Case 5. In the parameter space region

$$\tau_R<-(1+\delta_R), \quad \tau_L<0,$$

initial conditions in L move to R and vice versa. Therefore, the dynamics is governed by the stability of the second iterate with one point in L and the other in R.

The eigenvalues of the second iterate are

$$\tfrac{1}{2}(\tau_L\tau_R-\delta_R-\delta_L \pm \sqrt{\tau_L^2\tau_R^2-2\,\tau_L\tau_R\delta_R-2\,\tau_L\delta_L\tau_R+\delta_R^2-2\,\delta_R\delta_L+\delta_L^2}).$$

From this, the condition of stability of the period-2 orbit is obtained as

$$1-\tau_L\tau_R+\delta_L+\delta_R+\delta_L\delta_R>0 \quad \text{for} \quad \lambda_1<+1, \quad (12)$$

$$1+\tau_L\tau_R-\delta_L-\delta_R+\delta_L\delta_R>0 \quad \text{for} \quad \lambda_2>-1. \quad (13)$$

There are three subcases:

Case 5(a). If

$$\tau_R<-(1+\delta_R), \quad \tau_L<-2\sqrt{\delta_L},$$

and

$$1-\tau_L\tau_R+\delta_L+\delta_R+\delta_L\delta_R>0,$$

then there is a unique period-1 attractor for $\mu<0$ and a unique period-2 attractor for $\mu>0$.

For $\mu<0$, L^* is a flip attractor and $\bar{R}^*$ is a flip saddle. All initial conditions in L converge on L^* and all initial conditions in R go to L in the first iteration and then converge on to L^*. For $\mu>0$, the condition (12) ensures the stability of the period-2 orbit. The existence of heteroclinic intersection makes the attractor unique.

This is like a period-doubling bifurcation occurring on the borderline. In contrast with standard period-doubling bifurcation, the distinctive feature of the border collision period doubling is that as μ is varied through zero, the bifurcated orbit does not emerge orthogonally from the orbit before the bifurcation.

Case 5(b). If

$$\tau_R<-(1+\delta_R), \qquad -2\sqrt{\delta_L}<\tau_L<0,$$

and

$$1-\tau_L\tau_R+\delta_L+\delta_R+\delta_L\delta_R>0,$$

then for $\mu<0$ there can be multiple attractors, one of which is a period-1 fixed point. For $\mu>0$, the period-2 orbit involving both L and R is stable. Therefore, there is a unique period-2 attractor.

Case 5(c). If

$$\tau_R<-(1+\delta_R), \quad -(1+\delta_L)<\tau_L,$$

and

$$1-\tau_L\tau_R+\delta_L+\delta_R+\delta_L\delta_R<0,$$

then there is a period-1 attractor for $\mu<0$. For $-(1+\delta_L)<\tau_L<-2\sqrt{\delta_L}$, the eigenvalues of L^* are real and coexisting attractors cannot occur. Otherwise multiple attractors may exist. For $\mu>0$, since Eq. (12) is not satisfied, it implies that the fixed point of the twice iterated map is unstable. Its eigenvalues are real and initial conditions diverge away from it along the unstable eigenvector. Therefore, there can be no attractor for $\mu>0$.

Case 5(d). If

$$\tau_L<-(1+\delta_L), \quad \tau_R<-(1+\delta_R),$$

there is no attractor for both positive and negative values of μ since all the fixed points of the first and second iterate are unstable.

Case 6. Spiral attractor to flip saddle: This occurs if

$$0<\tau_L<2\sqrt{\delta_L}, \quad \tau_R<-(1+\delta_R).$$

For $\mu<0$, there can be multiple attractors, one of which is a period-1 fixed point. The asymptotic behavior for $\mu>0$ may be a periodic attractor (of periodicity greater than unity), or chaotic attractor. As τ_L is increased, periodic windows of successively higher periodicities (2,3,4, . . .) occur, and there are windows of chaos between two such periodic windows. The period-n attractor comes into existence through a border collision pair bifurcation in the nth iterate and goes out of existence when the period-n fixed point becomes unstable. The stability boundary of period-2 attractor is given by $1+\tau_L\tau_R-\delta_L-\delta_R+\delta_L\delta_R=0$. For higher iterates such analytical expressions for the boundary of periodic windows become involved and are not presented here. There is no mechanism to prevent the occurrence of multiple attractors.

This gives a complete description of the bifurcations that can occur at various regions of the parameter space of the normal form (5). Representative bifurcation diagrams of the cases (where attractors exist) are shown in Fig. 8.

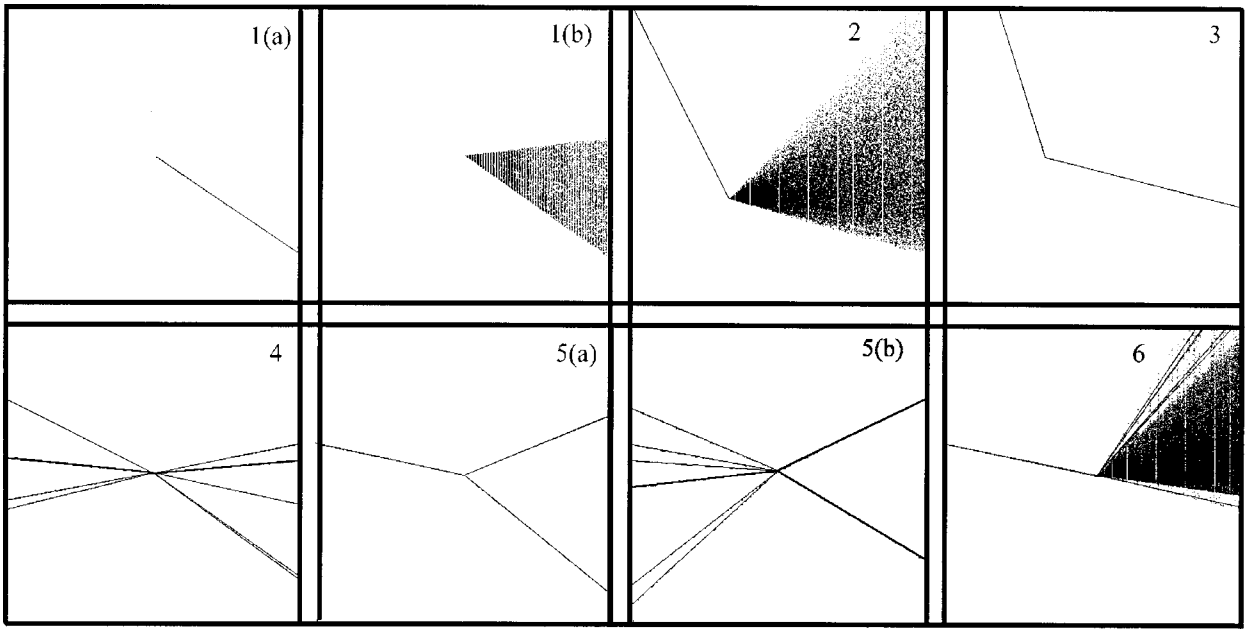

FIG. 8. Representative bifurcation diagrams of the normal form when μ is varied from a negative value to a positive value. For the cases where multiple attractors can exist, only one of many possibilities is shown. *Case 1(a),* no attractor to period-1 attractor; *Case 1(b),* no attractor to chaos; *Case 2,* period-1 to chaos; *Case 3,* period-1 to period-1; *Case 4,* period-1 + period-3 coexisting attractors to period-1 + period-4 coexisting attractors; *Case 5(a),* period-1 to period-2; *Case 5(b),* period-1 + period-11 coexisting attractors to period-2 attractor; *Case 6,* period-1 to coexisting period-5 + chaotic attractors.

C. The case of negative determinant

If the determinant is negative, one has to find out which type of fixed-point changes to which type as it moves across the border. Depending on the type of the fixed point at the two sides of the border, the bifurcations will be of the same kind as discussed in the previous section. For example, if $\delta_L, \delta_R < 0$, then the eigenvalues are real for all values of τ_L and τ_R. Therefore, there can be no coexisting attractors anywhere in the parameter space. The region of stability of period-2 attractor, given by conditions (12) and (13), is much larger. Moreover, there is a region of parameter space where a border collision pair bifurcation results in the creation of a period-2 attractor since condition (13) is satisfied. The partitioning of the parameter space for negative determinants is given in Fig. 9.

There is, however, a difference in the equation for the boundary crisis in border collision pair bifurcation. For $-1 < \delta_R < 0$, we have $1 > \lambda_{1R} > 0$, $\lambda_{2R} < -1$, and R^* is located above the x axis. A positive value of λ_{1R} implies that $\mathbf{U}_L$ converges on $\mathbf{U}_R$ from one side. If

$$\frac{\lambda_{1L}-1}{\tau_L-1-\delta_L} > \frac{\lambda_{2R}-1}{\tau_R-1-\delta_R}, \tag{14}$$

then the intersection of $\mathbf{U}_L$ with the x axis remains the rightmost point of the attractor and Eq. (11) still gives the parameter range for boundary crisis. But if Eq. (14) is not satisfied, the intersection of $\mathbf{U}_R$ with the x axis becomes the rightmost point of the attractor, and the condition of existence of the chaotic attractor changes to

$$\frac{\lambda_{2R}-1}{\tau_R-1-\delta_R} < \frac{\delta_L(\tau_L-\delta_L-\lambda_{2L})}{(\tau_L-1-\delta_L)(\delta_R\lambda_{2L}-\delta_L\tau_R)}. \tag{15}$$

For $\delta_L < 0$ and $\delta_R < 0$, L^* is below the x axis and the same logic as above applies. But if $\delta_L < 0$ and $\delta_R > 0$, the stable manifold of R^* has a negative eigenvalue and hence, $\mathbf{U}_L$ does not approach $\mathbf{U}_R$ from one side. Therefore, if Eq. (13) is not satisfied, there is no analytic condition for boundary crisis — it has to be determined numerically.

V. CONCLUSIONS

In this paper we have investigated the various types of border collision bifurcations that can occur in piecewise smooth maps by deriving a piecewise affine approximation of the map in the neighborhood of the border. We have shown that there can be basically eleven different types of border collision bifurcations, classified under six ''cases.'' We have presented a partitioning of the parameter space into regions where qualitatively different bifurcations occur.

This body of knowledge helps us in explaining the bifurcations observed in experimental and numerical investigations of switching circuits, some of which have been presented in Sec. II. For example, the experimental bifurcations of the type seen in Fig. 2 can occur in Case 2 and in a part of Case 6. A period-doubling bifurcation of the type shown in Fig. 3 can occur in the second iterate of the map if the parameters fall under Cases 5(a), 5(b), and a part of Case 6 (coexisting attractors cannot be observed in experimental bifurcation diagrams). The sudden appearance of a chaotic attractor as in Fig. 4 can occur in border collision pair bifurcation and can be categorized under Case 1(b). Note that this bifurcation occurs in the third iterate while the period-1 at-

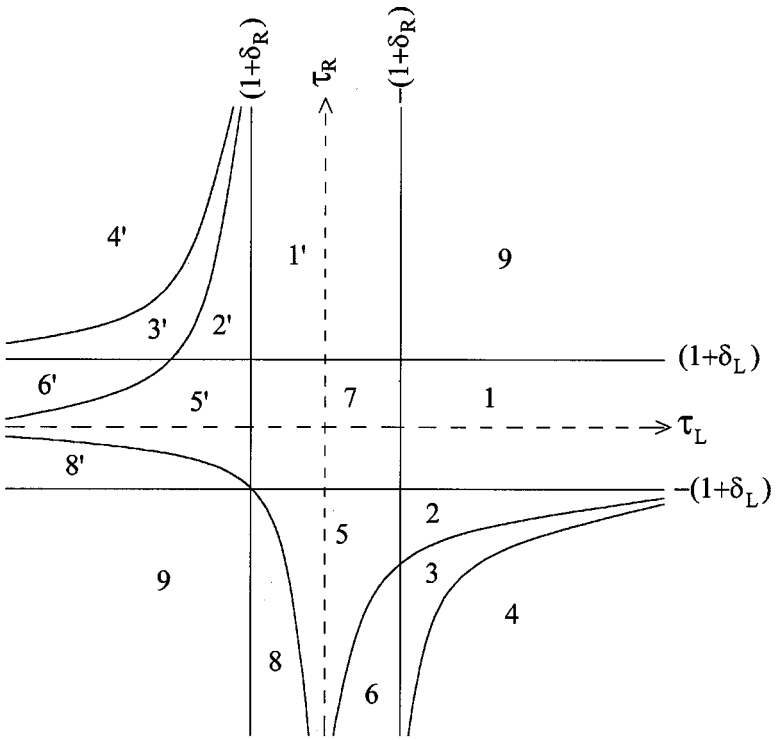

FIG. 9. Schematic diagram of the parameter space partitioning for $-1<\delta_L<0$ and $-1<\delta_R<0$ into regions with the same qualitative bifurcation phenomena. (1) No fixed point to period-1; (2) no fixed point to period-2; (3) no fixed point to chaos; (4) no fixed point to unstable chaotic orbit, no attractor; (5) period-1 to period-2; (6) period-1 to chaos; (7) period-1 to period-1; (8) period-1 to no attractor; (9) no attractor to no attractor. The regions shown in primed numbers have the same bifurcation behavior as the unprimed ones when μ is varied in the opposite direction.

tractor is present, and therefore, the resulting chaotic attractor is not robust.

The theoretical problem dealt in this paper was posed by the recent investigations in switching electrical circuits, but we believe that such atypical bifurcations will be observed in other nonsmooth physical systems also and the theory developed in this paper will help in understanding the nonlinear phenomena and bifurcations in such systems.

ACKNOWLEDGMENTS

We acknowledge the discussions with Professor J. A. Yorke and Dr. G. H. Yuan in the initial stages of this paper and the help provided by Dr. D. Kastha and Mr. S. Das in obtaining the experimental results. This paper was partly supported by NSF-CNPq, USA and by III 4(23)/94-ET, DST, India.

[1] W. Chin, E. Ott, H. E. Nusse, and C. Grebogi, Phys. Rev. E **50**, 4427 (1994).
[2] W. Chin, E. Ott, H. E. Nusse, and C. Grebogi, Phys. Lett. A **201**, 197 (1995).
[3] E. H. Nusse, E. Ott, and J. A. Yorke, Phys. Rev. E **49**, 1073 (1994).
[4] C. Budd and F. Dux, Philos. Trans. R. Soc. London, Ser. A **347**, 365 (1994).
[5] E. H. Nusse and J. A. Yorke, Physica D **57**, 39 (1992).
[6] S. Banerjee, E. Ott, J. A. Yorke, and G. H. Yuan, in *IEEE Power Electronics Specialists' Conference* (IEEE, New York, 1997), pp. 1337–1344.
[7] G. H. Yuan, S. Banerjee, E. Ott, and J. A. Yorke, IEEE Trans. Circuits Syst., I: Fundam. Theory Appl. **45**, 707 (1998).
[8] J. H. B. Deane and D. C. Hamill, IEEE Trans. on Power Electronics **5**, 260 (1990).
[9] D. C. Hamill, in *Nonlinear Dynamics of Electronic Systems*, edited by M. P. Kennedy (University College, Dublin, 1995).
[10] D. C. Hamill and J. H. B. Deane, IEEE Transactions on Power Electronics **7**, 25 (1992).
[11] C. K. Tse and W. C. Y. Chan, in *Power Electronics Specialists' Conference* (IEEE, New York, 1995).
[12] M. Ohnishi and N. Inaba, IEEE Trans. Circuits Syst., I: Fundam. Theory Appl. **41**, 433 (1994).
[13] I. Zafrany and S. Ben-Yaakov, in *Power Electronics Specialists' Conference* (Ref. [11]), pp. 1111-1117.
[14] S. Banerjee, J. A. Yorke, and C. Grebogi, Phys. Rev. Lett. **80**, 3049 (1998).
[15] J. H. B. Deane, IEEE Trans. Circuits Syst., I: Fundam. Theory Appl. **39**, 680 (1992).
[16] W. C. Y. Chan and C. K. Tse, in *Power Electronics Specialists' Conference*, edited by editors (IEEE, New York, 1996), pp. 789–795.
[17] S. Banerjee, IEEE Trans. Circuits Syst., I: Fundam. Theory Appl. **44**, 847 (1997).
[18] K. T. Alligood, T. D. Sauer, and J. A. Yorke, *Chaos: an Introduction to Dynamical Systems* (Springer, Berlin, 1996).